Long-term Impacts of Partial Afforestation on Water and Salt Dynamics of an Intermittent Catchment under Climate Change

Hossein Daneshmand [1], Sina Alaghmand [2,*], Matteo Camporese [3], Amin Talei [1], Pat J.-F. Yeh [1] and Edoardo Daly [2]

[1] Discipline of Civil Engineering, School of Engineering, Monash University Malaysia, Bandar Sunway, Selangor Darul Ehsan 47500, Malaysia; hosseindany@gmail.com (H.D.); Amin.Talei@monash.edu (A.T.); Pat.Yeh@monash.edu (P.J.-F.Y.)

[2] Department of Civil Engineering, Monash University, 23 College Walk, Clayton, VIC 3800, Australia; edoardo.daly@monash.edu

[3] Department of Civil, Environmental and Architectural Engineering, University of Padova, 35122 Padova, Italy; matteo.camporese@unipd.it

* Correspondence: sina.alaghmand@monash.edu

Abstract: Soil salinization is a major environmental issue in arid and semi-arid regions, and has been accelerated in some areas by removal of native vegetation cover. Partial afforestation can be a practical mitigation strategy if efficiently integrated with farms and pastures. Using an integrated surface-subsurface hydrological model, this study evaluates the water and salt dynamics and soil salinization conditions of a rural intermittent catchment in the semi-arid climate of southeast Australia subjected to four different partial afforestation configurations under different climate change scenarios, as predicted by several general circulation models. The results show that the locations of afforested areas can induce a retarding effect in the outflow of groundwater salt, with tree planting at lower elevations showing the steadier salt depletion rates. Moreover, except for the configuration with trees planted near the outlet of the catchment, the streamflow is maintained under all other configurations. It appears that under both Representative Concentration Pathways considered (RCP 4.5 and RCP 8.5), the Hadley Centre Global Environmental Model represents the fastest salt export scheme, whereas the Canadian Earth System Model and the Model for Interdisciplinary Research on Climate represent the slowest salt export scheme. Overall, it is found that the location of partial afforestation generally plays a more significant role than the climate change scenarios.

Keywords: dryland salinity; partial afforestation; climate change; intermittent catchments; MIKE SHE

1. Introduction

Soil salinization, which affects large parts of land in arid and semi-arid climatic zones worldwide, is related to the accumulation of water-soluble salts near the ground surface that negatively affect vegetation, with consequent reductions in ecosystem and agricultural productivity [1–3]. Salinization often occurs in areas with shallow or rising groundwater tables that allow salt-rich water to interfere with the rooting zone to the possible detriment of the land cover [4,5].

Land-use changes involving the replacement of deep-rooted trees with crops or pasture with shallow root system can result in soil salinization as well as water logging [6–8]. As changes in groundwater recharge patterns as a consequence of native vegetation loss play an essential role in the development of salinized drylands, numerous studies have investigated the re-introduction of

trees into the landscape as a form of mitigation strategy. While the establishment of large-scale plantations have been shown to lower the water table levels [9–11], they dramatically change the land use. With the attempt to maintain the agricultural production of the landscape, the integration of tree belts or tree blocks within farmlands has seen positive results in terms of groundwater recharge reductions without generating competitions for water resources between trees and crops or pastures [12–14]. In a study in southeast of Australia, van Dijk et al. [15] showed the efficiency of afforestation to mitigate river salinity and the potential of afforested areas to be increased by more than an order of magnitude through efficient spatial planning.

The expansion rate of dryland salinization worldwide is expected to increase due to climate change mainly because of the expansion of drylands [5]. In an analysis based on indicators established with a geographical information system (GIS) model, Schofield and Kirkby [16] discussed the possible generation of new areas across the world affected by salinization towards the end of the century. Kasim et al. [17] incorporated GIS and remote sensing (RS) with partial least squares regression models to monitor and predict spatial-temporal patterns of soil salinization in arid and semiarid regions. In a recent study, Erkin et al. [18] used machine learning and RS methods for predicting soil salinity in highly vegetated, and slightly and moderately salt-affected croplands.

Process-based hydrological models are still under-used for the prediction of possible effects of climatic changes on salt discharge, although being able to simulate processes affecting groundwater recharge more precisely than simple conceptual models [8,19–23]. Process-based models might provide useful insights on the response of catchments to change in climatic patterns [24–27]. With reliable climate-change projections and precise groundwater recharge estimations, process-based models can be used to quantitatively investigate the impacts of climate change on groundwater resources [28], a research issue which has attracted only limited attention so far [29]. At the regional scale, the potential effects of climate change on groundwater resources can be studied by combining hydrologic models and climate projection data downscaled from General Circulation Models (GCMs) simulations [30–32].

This study is a follow up to Daneshmand et al. (2019), where MIKE SHE, an integrated surface–subsurface hydrological model (ISSHM), was successfully calibrated and validated in the same catchment. However, Daneshmand et al. did not investigate different patterns of land use. In the present study, our main aim is to investigate the potential impacts that land use change, here represented as partial afforestation of a catchment originally covered by pasture, might have on the water balance and salt discharge under different climate-change scenarios. The physically-based model MIKE SHE was coupled to several statistically downscaled GCMs based on the resulting salt export rates, namely fastest and slowest salt export schemes. This work presents an example of applications of a well-established physically based hydrological model to investigate dryland salinity at the catchment scale and provides useful insights toward the long-term sustainability of partial afforestation of agricultural catchments.

2. Methods

This study builds upon the modelling work presented by Daneshmand et al. [20], where the model MIKE SHE was successfully applied for the simulation of water and salt fluxes in an intermittent stream catchment. MIKE SHE is a physically-based, fully integrated model capable of simulating the coupled surface water and groundwater interactions as well as salt transport and evapotranspiration at the catchment scale [33]. Following Daneshmand et al. [20], MIKE SHE was selected due to its adequate representation of the coupled physical processes as well as its computational efficiency and stability. In this study, MIKE SHE is combined with GCMs results to study the effect of climatic trends and partial afforestation on the water and salt balances. GCM outputs are downscaled using the LARS-WG [34,35] weather generator based on statistics obtained from historical weather data. Then, the resulting weather projections for each RCP and each representative GCM are used as inputs into MIKE SHE along with pre-defined plantation scenarios (see Figure 1).
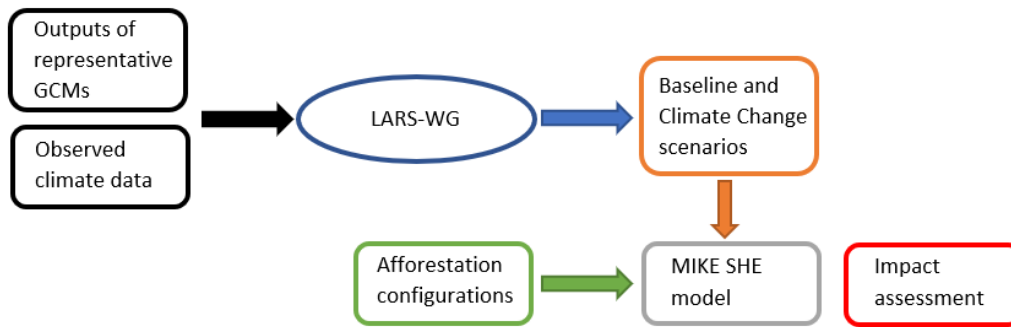
Figure 1. Workflow of impact assessment of the partial afforestation in combination with climate change projections.

2.1. Study Site

The study site, located near the town of Mirranatwa in southwest Victoria, Australia, is a small catchment (0.48 km^2) covered mainly by grass for grazing sheep (Figure 2). The long-term mean annual precipitation is 661.8 mm and the mean annual standardized reference evapotranspiration (ET_0) is 1070 mm. The subsurface is mainly alluvial/colluvial regolith weathered to varying extents for the top 7 m and fractured granite bedrock underneath [10,36].
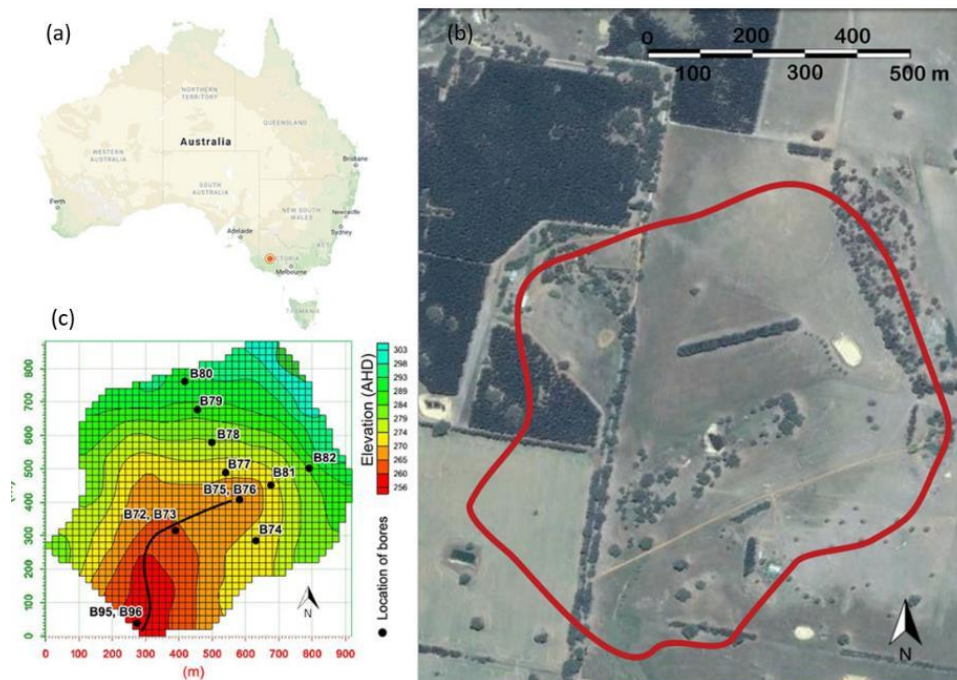
Figure 2. (**a**) Location of the catchment near Mirranatwa in southwestern Victoria, Australia. (**b**) Catchment boundaries, delineated by the solid red line, and land use (sourced from Google Earth). (**c**) Topography of the catchment, with black dots indicating the locations of groundwater bores and the black lines depicting the creek.

The monthly time series of ET_0 were calculated through the FAO-56 method [37] using the climate forcing data from the SILO database (http://www.longpaddock.qld.gov.au/silo) of the Queensland Climate Change Centre of Excellence. Daily precipitation data were obtained from the weather station 089019 maintained by the Bureau of Meteorology and located 2 km to the south of the catchment.

2.2. Hydrologic and Salt Transport Model

The MIKE SHE model setup as well as the calibration and evaluation of the model for the water and salt fluxes, were provided by Daneshmand et al. [20]. Thus, only a brief summary of the model is provided here. The parameters of surface and subsurface hydrologic processes were obtained from previous studies conducted at the same site [36,38,39] as listed in Table 1. The catchment digital elevation model was used to define the catchment finite-difference grid with a 20 m × 20 m cell size. The top 2 m of the soil within the domain was considered as the unsaturated zone (UZ) and discretized into 16 layers with an exponentially increasing thickness from the ground surface down to the water table. The saturated zone (SZ), from the water table at 2 m depth down to 10 m, was divided into 5 layers due to the significant reduction in the subsurface permeability at higher depths. An impermeable boundary condition was assumed for the bottom and lateral boundaries of the model domain as suggested by Dean et al. [36]. For the salt transport, flux boundary conditions were assigned at the surface, to define the salt inputs from precipitation, and at the bottom, to describe the decomposition of bedrock and regolith [20]. The initial condition of the model was generated using a 10-year warm-up period of precipitation and ET_0 data prior to 2011. The initial salinity condition was defined using a raster salinity map based on the measurements at 8 observational bores within the catchment. The model was calibrated and evaluated in the period between February 2011 and February 2013 against in-situ observed water and salt discharges and groundwater levels at the bores B74, B76, and B96 (Figure 2; see also Daneshmand et al., [20]).

Table 1. Main parameters characterizing the soil, surface flow, transpiration (K&J stands for Kristensen and Jensen, 1975), and salt transport.

Parameter	Value
Saturated hydraulic conductivity (K_s)	$K_s = 1.01 \times 10^{-5} z^{-0.27}$ [m s^{-1}]
Specific storage (S_s)	1×10^{-3} [1 m^{-1}]
Specific yield (S_y)	0.095
Saturated water content (θ_s)	0.4
Moisture content at field capacity (θ_{fc})	0.309
Wilting point (θ_{wp})	0.049
Residual moisture content (θ_r)	0.03
Matric potential at field capacity (Ψ_{fc})	0.0061 MPa
Matric potential at wilting point (Ψ_{wp})	1.5538 MPa
Van Genuchten α	1.85 [1 m^{-1}]
Van Genuchten n	1.52
Manning number at channel (m)	10 [m$^{1/3}$ s^{-1}]
Manning number at slope (m)	1 [m$^{1/3}$ s^{-1}]
K&J *LAI* *	1.01
K&J *C1* *	0.34
K&J *C2* *	0.4
K&J *C3*	20 [mm day^{-1}]
K&J Root Extinction Depth (Z_r)	1 [m]
Root distribution factor (A_{root})	1 [m^{-1}]
Canopy storage coefficient (C_{int})	0.2 [mm]
Longitudinal Dispersivity (a_L)*	5 [m]
Transverse Dispersivity (a_T)*	0.5 [m]
Dispersion Coefficient (a_D)*	0 [m^{-2} s^{-1}]

* Parameter values obtained through model calibration as in Daneshmand et al. [20].

2.3. Configurations of Partial Afforestation

Eucalyptus globulus (blue gum) trees are native to Australia, and are often used in plantations because of their fast growth rates. Therefore, they represent a realistic option for afforestation projects in Australia [12,13]. Four configurations of partial afforestation were studied, each covering 25% of the total catchment area (S1, S2, S3, and S4) with varying distances from the creek (Figure 3). To obtain the plantation locations of these configurations, all the grid cells were ranked based on their elevations and then classified in four quartiles. The grid cells adjacent to the creek were removed before ranking in order to maintain an average plantation distance of 30 m from the river bank, in compliance with the regulation prohibiting the plantation near the streams [38]. The configuration of plantation in each scenario was defined in MIKE SHE by specifying ET parameters different from those in Table 1, which pertain to the pasture. The plantation root depth was specified as 4 m, as suggested by Dean et al. [36] for *Eucalyptus globulus* (blue gum) trees, and LAI was estimated to be 3.5 from dendrometric data using the allometric relationship from Pereira, *et al.* [40]. The land cover transformation was assumed abrupt, i.e., no gradual root growth, occurring right before February 2011.
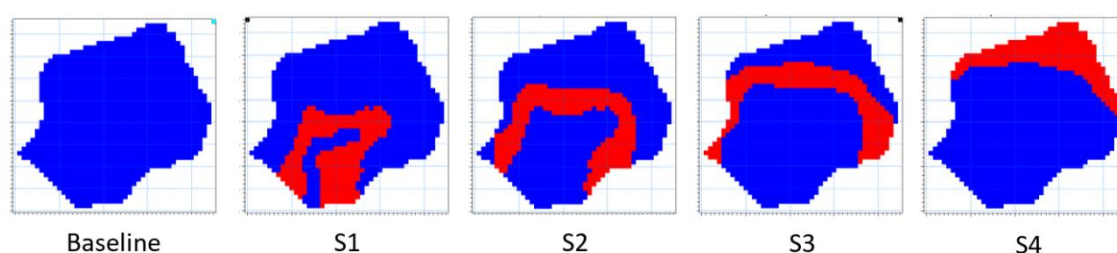
Figure 3. Configuration of the defined partial afforestation configurations: Baseline configuration with only the pasture cover for the entire catchment; S1, S2, S3 and S4 each with 25% plantation areas (in red), but varying locations and elevation.

2.4. Climate Change

2.4.1. GCMs to Represent Model Choice Uncertainty

The impacts of climate change on all the defined scenarios were investigated using GCM projection data as the input forcing data to the MIKE SHE model. The multi-purpose decision-support tool for impact assessment and adaptation planning, the Australian Climate Futures developed by CSIRO and Australian Bureau of Meteorology (www.climatechangeinaustralia.gov.au), was used to assess regional climate projections by changing two dominant climatic variables simultaneously, namely rainfall and ET_0. This tool consists of the statistically downscaled projection data from the GCMs participating in the Coupled Model Inter-comparison Project Phase 5 (CMIP5) [41] experiments that informed the Intergovernmental Panel on Climate Change (IPCC) Fifth Assessment Report [42]. In addition to accessing the GCM data at the regional grid size for each model, the data provided have also been downscaled from the CSIRO's Conformal-Cubic Atmospheric Model [43] and the Bureau of Meteorology statistical downscaling model [44].

Australian Climate Futures incorporated into the scenario design in this study was constructed based on CSIRO's RCP framework [45,46], which can be used to identify the proper models to represent the selected regional projections. The projections are classified by the combined changes in precipitation and ET_0. In this study, since the aim is to incorporate the impacts of partial afforestation and climate change to quantify catchment water and salt dynamics, the slowest salt export scheme is selected to be the projection with the largest increase in ET_0 and also the largest decrease in precipitation. On the other hand, the fastest salt export scheme is the one with the largest increase in precipitation and largest decrease in ET_0 occurring simultaneously.

As an initial requirement, the twelve months within one year were ranked based on the sensitivity of salt transport in each month to climate change, as will be explained in detail in the

following. To this end, we need to find the degree of the impacts that ET_0 and precipitation in each month have on the salt export rate, i.e., the sensitivity of the salt transport to monthly climate change factors. To estimate the monthly sensitivity, five years of precipitation and ET_0 data (2011–2016) were used to assess the relative change in modelled salt export as a result of a 30% increase in precipitation and ET_0. The flow and transport model was then run by changing one variable at one time for each of the twelve months of a year while keeping all other variables constant. The change in the exported salt at the end of the 5-year period was then divided by the total salt output of the base case where the afforestation was implemented. The calculated monthly sensitivity was then used to rank the monthly climate variables as the input to the Australian Climate Future online utility [47] to obtain the representative models under each climate change scenario considered.

2.4.2. Climate Scenarios Change Factors

The RCPs are characterized by the concentration of greenhouse emissions which will lead to specific amounts of radiative forcing in the year 2100. In this study, to achieve a comprehensive understanding of the future water and salt dynamics scenarios, RCP 8.5 and RCP 4.5 were chosen. The RCP 8.5 represents the pathway with the highest greenhouse gas emissions projected in the absence of climate change mitigation measures, and RCP 4.5 is associated with relatively ambitious programs of emission reduction [48]. The monthly data of climate change factors were available from the Australian Climate Futures online utility [49] for the scenario RCP 4.5, with the radiative forcing stabilized at 4.5 W m^{-2} in the year 2100 without ever exceeding that value, and RCP 8.5, with the radiative forcing stabilized at 8.5 W m^{-2} [50].

2.4.3. Downscaling Projections of Representative Models

The representative GCM outputs in the form of monthly change factors were downscaled to the daily timescale by using the Weather Generator (WG) approach for adequately describing future climate conditions in the study region. The LARS-WG [51,52] was used to calculate the probability distribution parameters of precipitation, solar radiation and daily temperature based on the daily observations as well as the correlations between them. These parameter sets can be used to produce synthetic weather time-series of any lengths by randomly selecting values from the appropriate distributions. The LARS-WG uses the historical climate data to identify the weather data distributions, which are described on a month-by-month basis through the semi-empirical, 45-parameter histogram-based models. Unlike the Markov chain-based stochastic weather generators, the model uses these histograms to generate precipitation independent of the length of the wet series or the amount of precipitation on the previous days. Therefore, it has the advantage of adequately modelling the alternating pattern of wet and dry series. The daily minimum and maximum temperatures are modelled based on the Fourier series of means and standard deviations conditioned on the precipitation status of the day [34]. The LARS-WG also accounts for the dependence of solar radiation to the wet or dry status of the day by implementing separate semi-empirical distributions for wet and dry days.

A 30-year (1986–2016) period with the recorded weather data was used to train the LARS-WG. The change factors provided by the representative GCMs in the CMIP5 Project were used to generate weather data for the time span of 92 years. The selection of a subset of GCMs is necessary due to computational, time, and resource constraints. In this study, three GCMs were selected to ensure that they capture a large range of the variability in climate outcomes observed across the entire ensemble from CMIP5. As denoted in Table 2, under RCP 4.5, the Canadian Earth System Model (CanESM2) [53] and the Hadley Centre Global Environmental Model version 2 (HadGEM2-CC) [54] were found to be representing fastest and slowest salt export schemes. For RCP 8.5, the Model for Interdisciplinary Research on Climate version 5 (MIROC5) [55] and the HadGEM2-CC were identified, respectively. The baseline climatology of all climate variables considered are summarized in Table 3.

Table 2. The change factors projected by the slowest and fastest salt transport schemes of the representative General Circulation Models (GCMs): the relative change in precipitation (ΔRain), the absolute changes in the minimum and maximum daily temperature (ΔT_{min}, ΔT_{max}), and the relative change in solar radiation (ΔSR). The baseline climatology is the long-term (1960–2016) mean values for each of the twelve months (as summarized in Table 3 below).

		RCP 4.5 Representative GCMs					
	CanEsm2 (Slowest)				HadGEM2-CC (Fastest)		
Month	ΔPrecipitation	ΔT_{min} (°C)	ΔT_{max} (°C)	ΔSR	ΔPrecipitation	ΔT_{min} (°C)	ΔT_{max} (°C)	ΔSR
January	0.98	1.78	1.59	0.99	1.17	1.71	2.06	1.01
February	0.85	1.84	1.34	1	1.08	1.48	1.7	1.02
March	0.86	1.74	1.28	1	0.92	1.82	2.07	1.01
April	1.07	1.65	1.9	1.02	1.05	1.31	1.38	1.01
May	0.87	1.12	1.2	1.02	1.03	1.7	2.15	1.02
June	0.85	0.92	0.89	1	1.06	1.39	1.66	1.04
July	0.93	1.11	1.27	0.99	1.04	1.47	1.74	1.01
August	0.98	1.1	1.21	0.99	1.11	1.1	1.4	1.03
September	0.97	1.13	0.99	0.98	1.32	1.55	1.8	1.02
October	0.98	0.89	1.03	1.01	0.91	1.65	2.01	1.02
November	0.99	0.99	1.54	1.03	0.85	1.67	2.04	1.02
December	1.01	1.11	1.2	1	0.93	2.31	2.55	1.01
		RCP 8.5 Representative GCMs					
	MIROC5 (Slowest)				HadGEM2-CC (Fastest)		
Month	ΔPrecipitation	ΔT_{min} (°C)	ΔT_{max} (°C)	ΔSR	ΔPrecipitation	ΔT_{min} (°C)	ΔT_{max} (°C)	ΔSR
January	0.97	1.3	1.51	1.01	1.01	1.61	1.88	1.02
February	1.1	1.31	1.41	1	1	1.78	1.83	1.02
March	0.92	1.03	1.3	1.03	1.03	2.4	3.03	1.05
April	1.08	1.13	1.18	1	1	2.21	2.25	1
May	1.04	1.19	1.24	1.01	1.01	2.02	2.37	1.02
June	0.97	1.39	1.6	1.02	1.02	1.88	2.19	1.05
July	1	1.39	1.48	1.02	1.02	1.49	1.72	1.01
August	1.01	1.11	1.29	1.03	1.03	1.43	1.51	1.01
September	0.98	1.35	1.59	1.01	1.01	1.62	1.75	1.01
October	0.82	1.21	1.55	1.03	1.03	1.62	1.96	1.02
November	0.9	1.16	1.5	1.01	1.01	1.81	2.29	1.03
December	1.07	0.95	0.96	0.99	0.99	2.27	2.45	1

Table 3. Average monthly climate data for the baseline period (1960 to 2016).

| Month	Precipitation (mm)	T_{min} (°C)	T_{max} (°C)
January	39.06	11.36	26.75
February	27.74	11.72	27.46
March	34.25	10.35	24.15
April	47.56	7.98	19.96
May	61.10	6.3	15.92
June	66.05	4.74	12.85
July	78.99	3.9	12.12
August	82.28	4.42	13.42
September	75.49	5.56	15.39
October	67.27	6.56	18.07
November	56.19	8.23	21.46
December	46.57	9.95	24.59

3. Results and Discussion

3.1. The Impacts of Partial Afforestation

To estimate the sole impact of the partial afforestation configurations and to exclude the climate change impacts on the catchment flow and salt transport regimes, it was assumed the climate stays the same for the study period. Thus, the MIKE SHE model was run using the 4-year (February 2011 to February 2015) climate forcing data and then it was extended for 23 cycles to produce an overall 92 years of simulation, corresponding to a projected period from year 2016 to 2107.

3.1.1. Water Balance

Figure 4 shows the simulated responses of catchment discharge to the partial afforestation scenarios. Due to the influence of the initial conditions, the differences in catchment discharge among all the scenarios are negligible for the first year, while in the following years the reduction in discharge becomes evident. The extent of the reduction is generally proportional to the discharge rate, with the peak discharge mostly affected. Trees reduce the water table levels at the planted locations by increasing ET from the groundwater (see ET_{sz} in Table 4). For the scenario S1, the water table where the trees are located is shallow; therefore, a lowered water table level, due to increased transpiration, can have more significant influences on both the extent and frequency of the groundwater-stream connectivity. For S4, however, the full saturation of the soil is unlikely due to the deeper water table in the plantation location, and thus the discharge rate is controlled by the ability of the trees to reduce the hydraulic gradient.
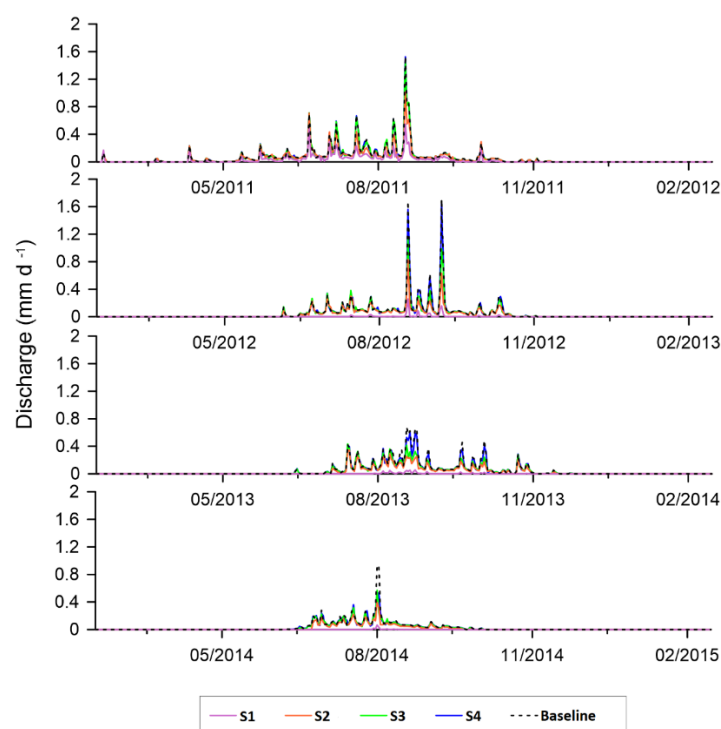
Figure 4. Simulated catchment discharge flow under the baseline and four partial afforestation scenarios between February 2011 and February 2015.

Table 4. Comparisons of the mean changes in water balance components from Feb 2011 to Feb 2015.

Water Balance Components (mm/y)	S1	S2	S3	S4	Baseline
Δs (SZ)	−14.04	−28.36	−37.80	−28.94	25.62
Δs (UZ)	−234.67	−268.58	−279.84	−269.13	−51.57
ET_{sz}	93.36	26.03	8.19	11	11.85

|					
D	11.87	48.78	60.58	67.36	70.56
ET	641.14	640.67	640.01	635.89	579.67

Δs: storage change for saturated (SZ) and unsaturated (UZ) zones, ET_{sz}: direct evapotranspiration from groundwater, D: catchment discharge, ET: total evapotranspiration.

The distribution of water balance components under all four partial afforestation scenarios are listed in Table 4. There is a rather steady decrease in the total stream discharge at the end of the 4-year period as the partial afforestation moves downhill towards the catchment outlet, and this reduction is very large in the lowland plantation configuration (S1). Total ET is similar for S1 to S3 configurations, whereas in S4 the relatively lower total ET suggests lower moisture availability. With similar ET values, S3 has the largest loss of subsurface storage after the transition (Δs in SZ and UZ) because this configuration alters the aquifer-stream connectivity the least, and hence discharge remains uninterrupted. Thus, the subsurface water storage is preserved better in S1 and S2 configurations.

3.1.2. Salt Balance

To observe the long-term behavior in the salinity trends, the flow simulation results during the four-year period were used as the basis to provide a 92-year simulation of salt transport by repeating the flow vectors, an artificial condition which assumes the climatic conditions similar to those in recent years. Figure 5 shows the salt export rate and the average salt concentration in the discharged streamflow throughout the simulated period. An overall reduction in the export rate of salt is evident as the location of partial afforestation moves downslope.

(**a**)

(**b**)
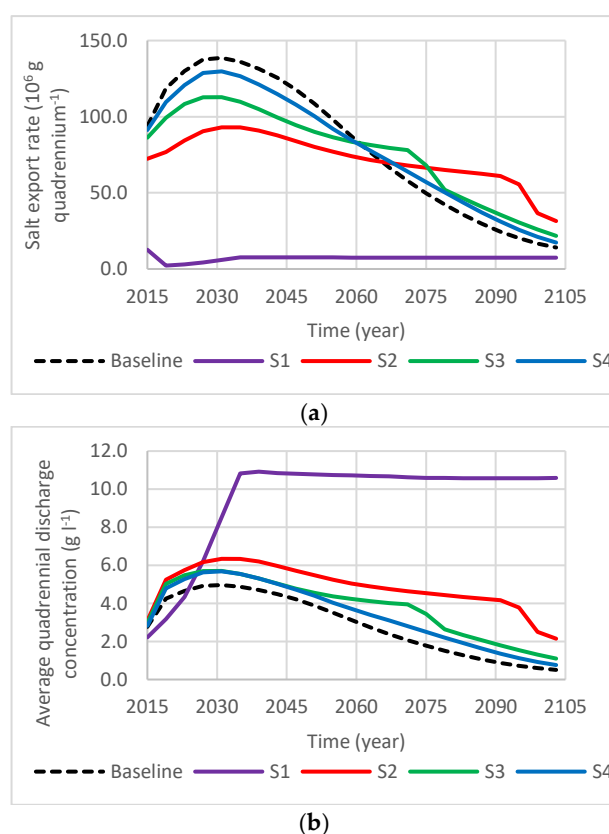
Figure 5. Simulated salt export rate (**a**) and average salt concentration of discharge flow (**b**) per every 4 years since the start of simulation.

When part of the pasture is replaced by trees, transpiration significantly increases along the plantation area. Therefore, the upstream groundwater traveling towards the outlet would experience an increase in transpiration upon reaching the afforested area, which in turn leads to an increased salt accumulation. For instance, in the S2 configuration, compared to S3, a larger area of the aquifer

is located upslope, and, therefore, a larger supply of salt moves through the plantation area. As a result, the salt export rate is smaller in magnitude but lasts longer (36 years for S2 compared to 11 years for S3), followed by a sharp decrease when salt supplies from upslope areas ends. This is showed as a sudden drop in salt export rate in Figure 5 for S2 and S3 configurations. For the S3 configuration, where the afforested area is at upper elevations, the entire process occurs earlier, together with a larger export rate until this falls sharply in 2070. Salt export under both S2 and S3 configurations is slower and sustained longer than in S4, due to higher ET and lower discharge.

The S1 configuration shows an entirely different salt export trend as a result of the stream drying out. Afforestation in the vicinity of the creek significantly alters the surface water-groundwater connectivity, leading to very low streamflow with a consequent very small salt export and increase in salt concentration at the outlet (Figure 5b). In this configuration, over the first few years, as driven by the initial water heads there is a large salt discharge that decreases with the declining water table and the consequent reduction in surface water-groundwater connectivity. The constant salt export rate indicates that the maximum salt solubility is reached as a result of high local ET rates. In the S4 configuration, instead, the afforestation is established in the most upslope area of the catchment where the water table is at the deepest; therefore, the plantation does not increase the transpiration dramatically, resulting in a very small impact on the salt export compared to the baseline. Overall, these results indicate the important role played by the plantation location on both water and salt balance in seasonally dry catchments.

The favorable result of a reduction in the salt export is usually accompanied by a decrease in the streamflow discharge, which is unfavorable. Therefore, a function was defined to assess the benefits of each configuration as the difference between the relative change in salt export and the relative change in flow discharge, i.e.,

$$O_i = \frac{E_{Si} - E_B}{E_B} - \frac{D_{Si} - D_B}{D_B}, \tag{1}$$

where E_{Si} and D_{Si} are quadrennial salt export and flow discharge at the *i*th scenario. Therefore, a smaller O_i is desirable and a negative value means that there is a larger reduction in the exported salt than that in the discharge rate.

As shown in Figure 6, O_2 is the largest throughout the simulation period, in particular with a substantial rise in the second half of the period. For the first half of the simulation period, O is nearly unchanged across all configurations, whereas differences can be found mainly in the second half of the period when the S2 configuration exhibits a large increase corresponding to the salt accumulation which is consistent with Figure 5a. The value of O_1 remains near zero for the majority of the period as a result of generally no-flow conditions.
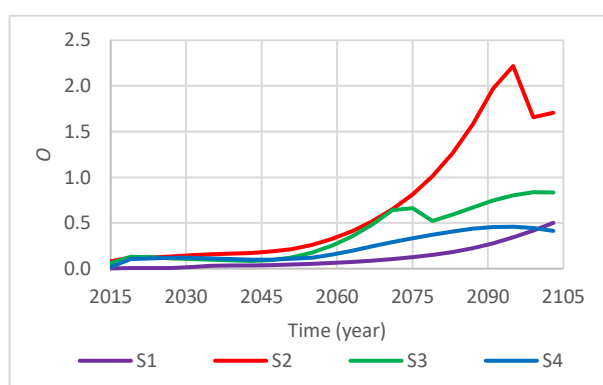

Figure 6. Objective function O (defined as the difference between the relative change in salt export rate and the relative change in catchment discharge rate relative to that in the baseline scenario, Equation (1) for the four different configurations considered.

It seems that the defined partial afforestation configurations are more disadvantageous than the baseline pasture cover from this perspective, with the exception of S1 with the plantation at the lowest

lying area. In this configuration, salt export and flow discharge rates both approach zero as shown in Figures 4 and 5.

3.2. Combined Impacts of Partial Afforestation and Climate Variability

The sensitivity of monthly salt export rates to the ET_0 and precipitation rates for each month is shown in Figure 7, which reports the sensitivity of the transport model to 30% variations in monthly precipitation and ET_0 in terms of percentage change in total exported salt. The overall transport rate is affected by the total recharge, which is in turn affected by precipitation and ET_0. As shown in Figure 7, the salt export rate increases with precipitation and decreases with ET_0, so the sensitivity is positive for precipitation and negative for ET_0. Overall, the transport model is more sensitive to the changes in precipitation than in ET_0, particularly during wet seasons. The highest sensitivity to ET_0 is in September and March, probably because of a combination of lower precipitation but large water availability to evapotranspiration during these months.
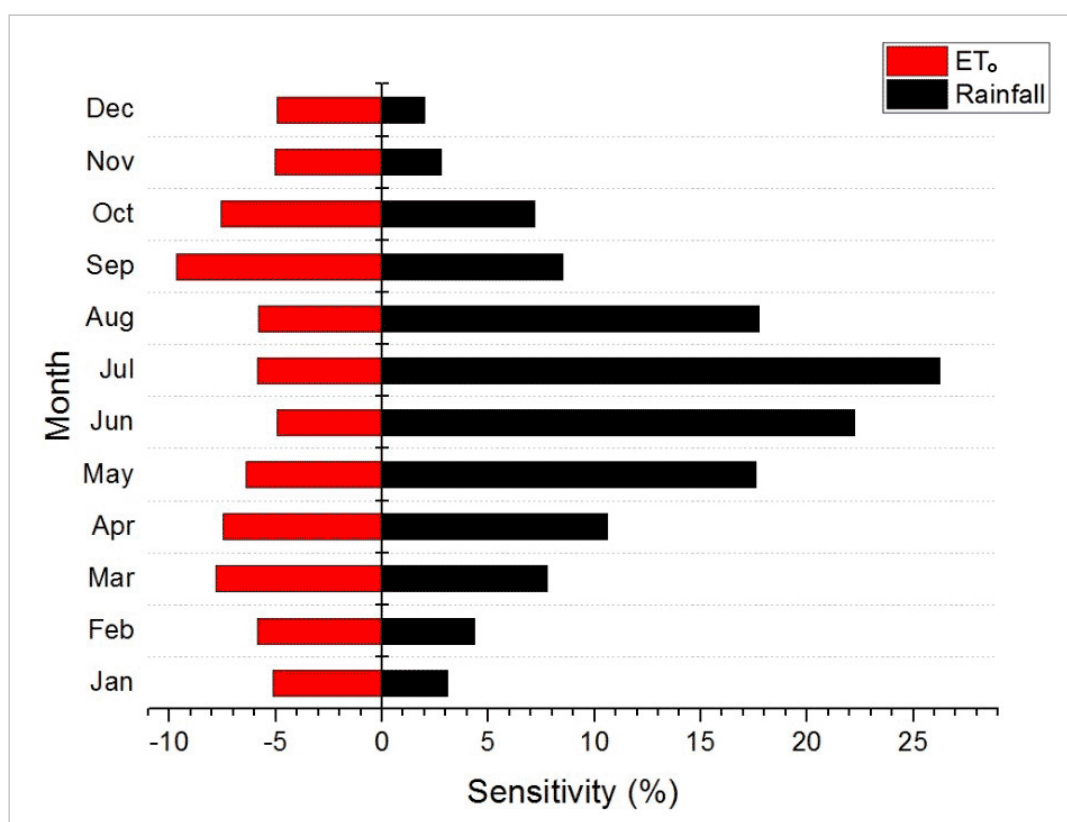
Figure 7. The sensitivity of the salt transport model to 30% variations in monthly ET_0 and Rainfall expressed as the percentage change in the total exported salt.

The ranking of the months of the year for precipitation and ET_0 based on these sensitivity levels is given in Table 5. The monthly sensitivities are thus ranked in order of importance based on the absolute magnitudes of sensitivity.

Table 5. Ranking of monthly precipitation and ET based on the sensitivity indices.

Month	Precipitation		ET_0	
	Sensitivity	Rank	Sensitivity	Rank
January	0.031	22	−0.051	17
February	0.043	21	−0.059	14
March	0.078	9	−0.078	8
April	0.106	5	−0.075	11
May	0.176	4	−0.064	13

June	0.222	2	−0.049	19
July	0.263	1	−0.059	15
August	0.177	3	−0.058	16
September	0.085	7	−0.097	6
October	0.072	12	−0.076	10
November	0.028	23	−0.050	18
December	0.020	24	−0.049	20

3.2.1. Impact on Catchment Salt Load

Simulated results of the cumulative salt export for S1–S4 configurations from two representative GCMs and the baseline case are shown in Figure 8 for both the RCP 4.5 and RCP 8.5 scenarios. The shaded area represents the range of the uncertainties from the choices of GCMs. Under the RCP 4.5 scenario, the baseline case stores slightly more solute mass than CanESM2, the fastest salt export scheme, but generally less than HadGem2-CC, the slowest salt export scheme. The S1 configuration is very different from all the others, which show a progressive reduction in salt export rate over time. In addition, the uncertainty range is wider than S2, S3, and S4, indicating that the salt export rate is most sensitive to climate uncertainty under the S1 configuration.
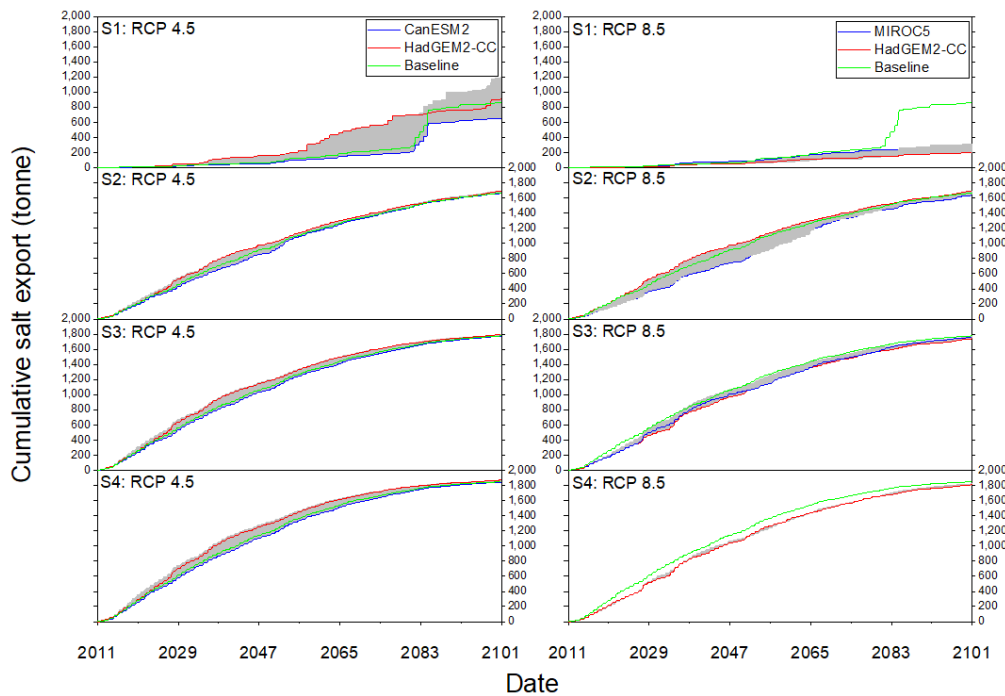

Figure 8. Cumulative salt export across the different partial afforestation configurations and RCP scenarios.

The S2 configuration shows a cumulative discharge curve with a smaller curvature compared to other configurations. As the salt export rate is smaller for S2, it is likely that not all the accumulated salts have left the catchment at the end of the simulation period, while in other configurations, especially S4, the curve tends to be flatter, indicating the termination of salt export. While the representative GCMs yield similar results under RCP 4.5, GCMs generally show a slower salt export compared to the baseline case under RCP 8.5. Results for the S3 and S4 configurations are rather similar in that both show a faster salt export rate than the baseline case under RCP 4.5 and a slower rate than the baseline case under RCP 8.5.

### 3.2.2. Impact on Top Soil Salinity

The mean salinity of the top 10-cm soil spatially averaged across the surface of the catchment is shown in Figure 9. Under both RCP scenarios, both S1 and S2 configurations have the peak salinity

occurring at a later time, and the peak salinity is slightly larger under RCP 8.5 for all configurations. These two configurations, particularly S1, result in more saline soil profiles on average. Under each RCP, the S4 and S3 configurations show the same peak values. However, the decay rate is larger for S4, resulting in a final soil salinity, under RCP 4.5, of ~600 mg L^{-1} for S3 and 500 mg L^{-1} for S4. A similar trend is observable under RCP 8.5 with both the peak and the final soil salinity being larger by ~100 mg L^{-1} compared to that under RCP 4.5.
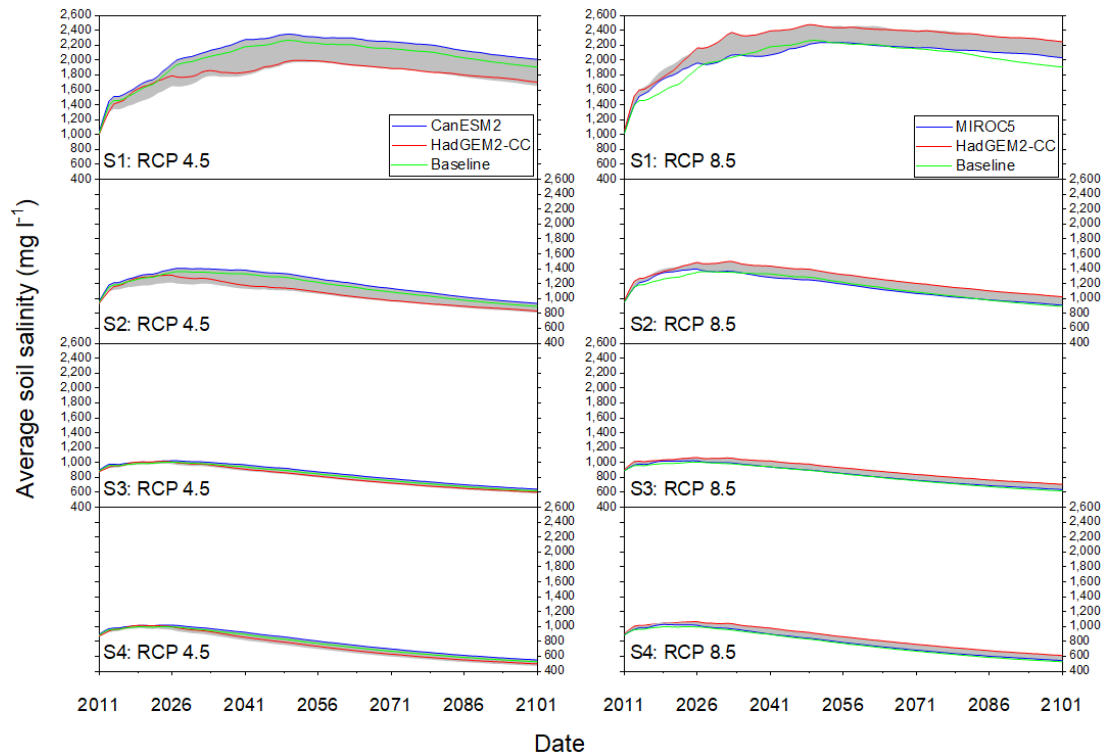

Figure 9. The average soil profile salinity across different partial afforestation configurations and RCP scenarios considered in this study.

For all the configurations under RCP 8.5, the simulation with the fast transport (HadGEM2-CC) is not associated with the lowest soil salinity. This is in contrast to that found under RCP 4.5, likely due to the larger projected ET_0 by this model resulting in a drier soil and hence larger salinity. Both overall soil salinity and uncertainty within GCMs decrease progressively from S1 to S4. Figure 10 depicts the 3D visualization of soil profile salinity simulations at the start and the end of the study period for the S3 configuration under RCP 4.5. A significant salt depletion is evident, as this is the scenario with overall the least solute mass accumulation and the highest salt export rate among the simulated scenarios, resulting in the least salinized area at the end of the study period (Figure 11).
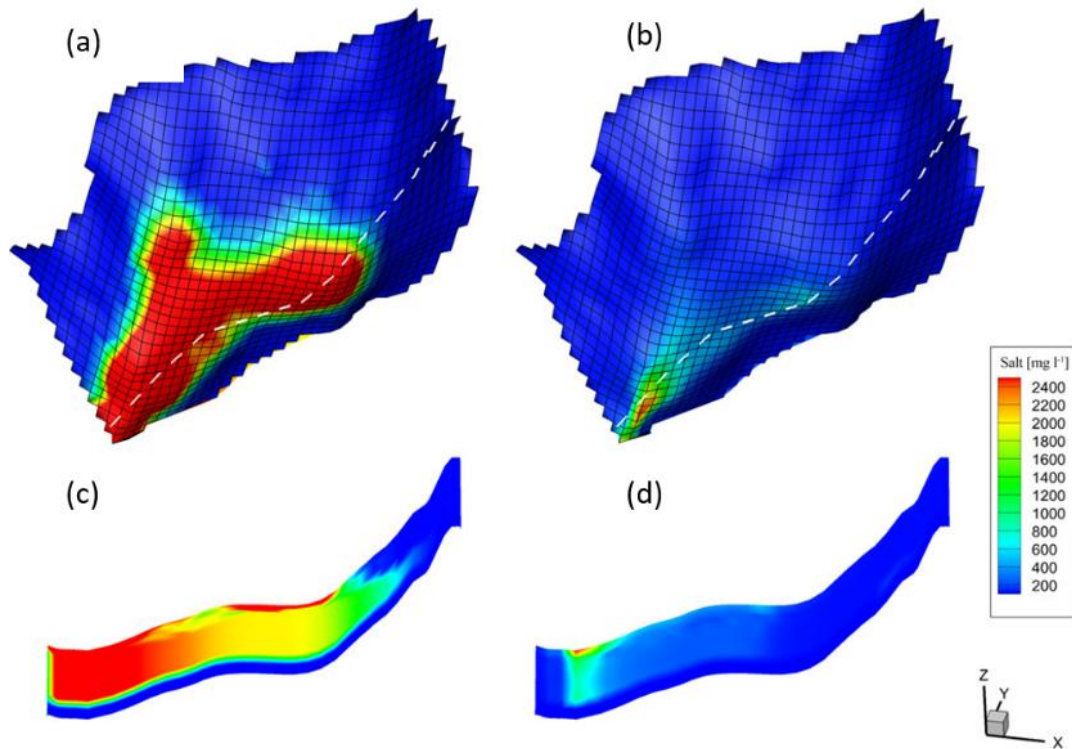
Figure 10. The 3D visualization of soil profile salinity simulations at the start (2011) (**a**) and the end (2107) (**b**) of the study period for the S3 configuration under RCP 4.5. (**c**) and (**d**) illustrate the soil profile salinity along the streams of the catchment (i.e., the white dashed line).
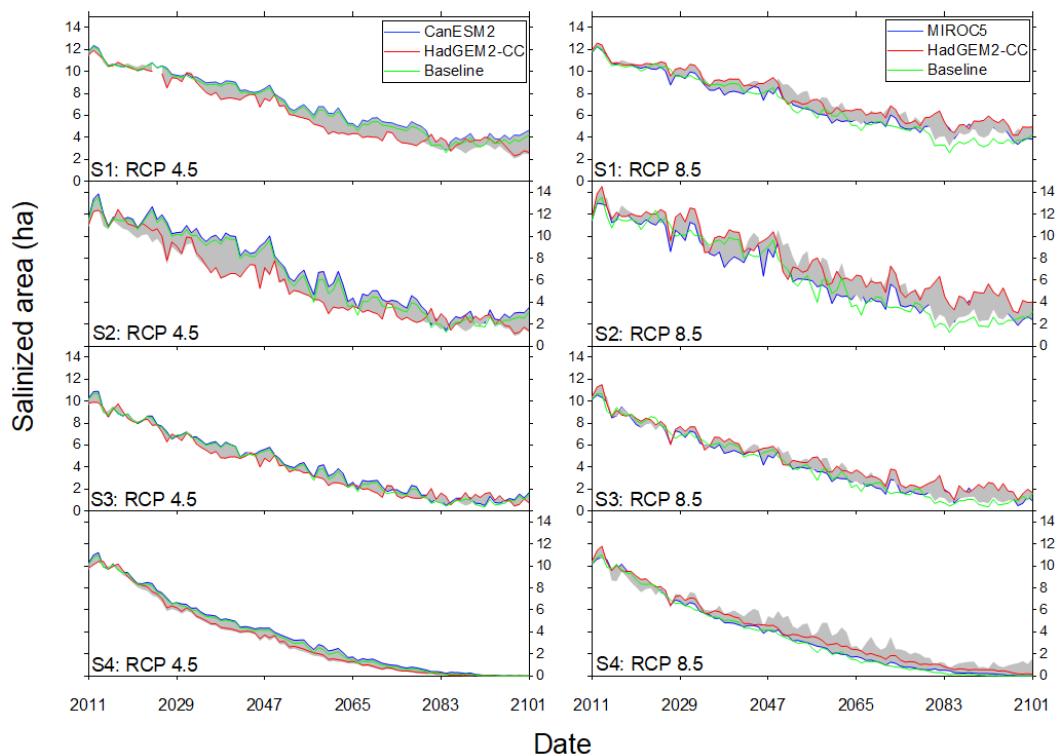
Figure 11. Total salinized area across different partial afforestation configurations and RCP scenarios.

3.2.3. Impact on Total Salinized Area

Salinized area is defined where the top 10 cm of soil is affected by a salt concentration larger than 2000 mg L^{-1} (Figure 11). Overall, the salinized area increases throughout the period when

moving the afforested area downslope and hence increasing the proximity of plant roots to the water table. In each individual configuration, this area decreases with the gradual salt depletion of the catchment over time. The S4 configuration has salinized area approaching zero faster than other configurations, and this is consistent among all representative GCMs. Under RCP 8.5, as a result of the larger maximum and minimum daily temperatures and thus larger ET_0, some areas remain salinized until the end of the study period regardless of the insignificant variation in salt export rate when compared to the afforestation configuration under RCP 4.5. Under RCP 8.5, this depletion rate is highest for the HadGem2-CC model; however, the salinized area shrinks faster for the MIROC5 model. This is again because of an overall larger projected ET_0 by MIROC5. The salinized area is always larger under RCP 8.5 in all configurations except S3.

4. Conclusions

Vegetation cover change, such as the removal of native vegetation in Australia for agricultural and pasture activities, may lead to significant changes in catchment water balances, resulting in the development of dryland salinization in arid and semi-arid regions. Therefore, it is necessary to quantitatively assess the potential impacts of partial afforestation spatial configurations that may improve salinity conditions without dramatically affecting streamflow. In addition to the common debate on the impacts of percentage of afforested area, this study evaluated the processes affected by partial afforestation under different climate-change scenarios. The MIKE SHE model was used here to quantify the impacts of partial afforestation on the water and salt dynamics under climate-change scenarios of a rural catchment in the semi-arid climate of southeast Australia. The results show that a partial afforestation established at the lower elevations, closer to the catchment outlet, exerts a stronger influence on the water and salt balance, whereby a closer proximity of trees to groundwater enhances root water uptake. Moreover, the locations of afforestation can induce a retarding effect in the outflow of groundwater salt, with the lower elevation configuration showing the steadier salt depletion rates. MIKE SHE also helped to identify the best GCMs for the assessment of climate change based on the system sensitivity to climate forcing in each month of the year. The combined simulations of partial afforestation and climate change reveal that, except for S1 with trees planted near the outlet of the catchment, the streamflow is maintained under all configurations. It appears that under both RCP 4.5 and RCP 8.5 scenarios, the HadGEM2-CC is the GCMs with the fastest salt export scenario, whereas the CanEsm2 and MIROC5 represent the slowest salt export scenarios. In terms of mean soil salinity and total salinized areas, the RCP 4.5 is the more ideal scenario while RCP 8.5 shows only slightly larger mean values than the baseline case. For the salt discharge rate, it is found that the location of partial afforestation generally plays a more significant role than the climate change scenarios or GCM choices.

Overall, our study demonstrates that partial afforestation might be used as an effective salinity management option, but it needs careful planning to be integrated within existing headwater catchments while maintaining the intermittent streamflow. It is shown that water and salt dynamics in arid and semi-arid intermittent catchments are highly sensitive to partial afforestation. It appears that for the same percentage of afforestation area, the spatial configuration plays an essential role in influencing long term salinity conditions. Moreover, with the objective to accelerate salt export, different combinations of climate change scenarios and partial afforestation configurations will lead to significantly different and sometimes adverse results. Therefore, where well-observed and data-rich catchment is available, ISSHM models are efficient tools to study such complex dynamics for each specific catchment. The findings of this study seem critical for water resources managers because they show that success of partial afforestation under climate change depends on consideration of its spatial configuration.

Author Contributions: Contribution of each author is as follows: H.D Data curation, Investigation, Writing Original Draft; S.A. Supervision, Methodology; M.C. Writing- review& editing, Funding acquisition; A.T. Supervision, Project administration; P.J.-F.Y. Writing- review& editing; E.D. Supervision, Writing- review& editing. All authors have read and agreed to the published version of the manuscript.

Conflicts of Interest: The authors declare no conflict of interest.

References

1. Dregne, H.E. Land degradation in the drylands. *Arid Land Res. Manag.* **2002**, *16*, 99–132, doi:10.1080/153249802317304422.

2. Alaghmand, S.; Beecham, S.; Hassanli, A. A review of the numerical modelling of salt mobilization from groundwater-surface water interactions. *Water Resour.* **2013**, *40*, 325–341.

3. Prǎvǎlie, R. Drylands extent and environmental issues. A global approach. *Earth Sci. Rev.* **2016**, *161*, 259–278, doi:10.1016/j.earscirev.2016.08.003.

4. Alaghmand, S.; Beecham, S.; Hassanli, A. Impacts of groundwater extraction on salinization risk in a semi-arid floodplain. *Nat. Hazards Earth Syst. Sci.* **2013**, *13*, 3405–3418, doi:10.5194/nhess-13-3405-2013.

5. D'Odorico, P.; Bhattachan, A.; Davis, K.F.; Ravi, S.; Runyan, C.W. Global desertification: Drivers and feedbacks. *Adv. Water Resour.* **2013**, *51*, 326–344, doi:10.1016/j.advwatres.2012.01.013.

6. Allison, G.; Cook, P.; Barnett, S.; Walker, G.; Jolly, I.; Hughes, M. Land clearance and river salinisation in the western Murray Basin, Australia. *J. Hydrol.* **1990**, *119*, 1–20.

7. Rengasamy, P. World salinization with emphasis on Australia. *J. Exp. Bot.* **2006**, *57*, 1017–1023, doi:10.1093/jxb/erj108.

8. Archibald, R.D.; Harper, R.J.; Fox, J.E.D.; Silberstein, R.P. Tree Performance and Root-Zone Salt Accumulation in Three Dryland Australian Plantations. *Agrofor. Syst.* **2006**, *66*, 191–204, doi:10.1007/s10457-005-6644-2.

9. Dresel, P.E.; Dean, J.F.; Perveen, F.; Webb, J.A.; Hekmeijer, P.; Adelana, S.M.; Daly, E. Effect of Eucalyptus plantations, geology, and precipitation variability on water resources in upland intermittent catchments. *J. Hydrol.* **2018**, *564*, 723–739, doi:10.1016/j.jhydrol.2018.07.019.

10. Adelana, S.M.; Dresel, P.E.; Hekmeijer, P.; Zydor, H.; Webb, J.A.; Reynolds, M.; Ryan, M. A comparison of streamflow, salt and water balances in adjacent farmland and forest catchments in south-western Victoria, Australia. *Hydrol. Process.* **2015**, *29*, 1630–1643.

11. White, D.A.; Dunin, F.X.; Turner, N.C.; Ward, B.H.; Galbraith, J.H. Water use by contour-planted belts of trees comprised of four Eucalyptus species. *Agric. Water Manag.* **2002**, *53*, 133–152, doi:10.1016/S0378-3774(01)00161-5.

12. Wildy, D.T.; Pate, J.S.; Bartle, J.R. Budgets of water use by Eucalyptus kochii tree belts in the semi-arid wheatbelt of Western Australia. *Plant Soil* **2004**, *262*, 129–149, doi:10.1023/B:PLSO.0000037058.85572.ba.

13. Brooksbank, K.; Veneklaas, E.J.; White, D.A.; Carter, J.L. Water availability determines hydrological impact of tree belts in dryland cropping systems. *Agric. Water Manag.* **2011**, *100*, 76–83, doi:10.1016/j.agwat.2011.08.016.

14. Van Dijk, A.I.J.M.; Gilfedder, M.; Austin, J. Influences of climate, terrain and land cover on stream salinity in southeastern Australia, and implications for management through reforestation. *Hydrol. Process.* **2008**, *22*, 3275–3284, doi:10.1002/hyp.6968.

15. Schofield, R.V.; Kirkby, M.J. Application of salinization indicators and initial development of potential global soil salinization scenario under climatic change. *Glob. Biogeochem. Cycles* **2003**, *17*, doi:10.1029/2002GB001935.

16. Kasim, N.; Tiyip, T.; Abliz, A.; Nurmemet, I.; Sawut, R.; Maihemuti, B. Mapping and Modeling of Soil Salinity Using WorldView-2 Data and EM38-KM2 in an Arid Region of the Keriya River, China. *Photogramm. Eng. Remote Sens.* **2018**, *84*, 43–52, doi:10.14358/PERS.84.1.43.

17. Erkin, N.; Zhu, L.; Gu, H.; Tusiyiti, A. Method for predicting soil salinity concentrations in croplands based on machine learning and remote sensing techniques. *J. Appl. Remote Sens.* **2019**, *13*, 034520.

18. Alaghmand, S.; Beecham, S.; Hassanli, A. Impacts of vegetation cover on surface-groundwater flows and solute interactions in a semi-arid saline floodplain: A case study of the lower Murray River, Australia. *Environ. Process.* **2014**, *1*, 59–71.

19. Alaghmand, S.; Beecham, S.; Jolly, I.D.; Holland, K.L.; Woods, J.A.; Hassanli, A. Modelling the impacts of river stage manipulation on a complex river-floodplain system in a semi-arid region. *Environ. Model. Softw.* **2014**, *59*, 109–126.

20. Daneshmand, H.; Alaghmand, S.; Camporese, M.; Talei, A.; Daly, E. Water and salt balance modelling of intermittent catchments using a physically-based integrated model. *J. Hydrol.* **2019**, *568*, 1017–1030, doi:10.1016/j.jhydrol.2018.11.035.

21. Alaghmand, S.; Beecham, S.; Woods, J.A.; Holland, K.L.; Jolly, I.D.; Hassanli, A.; Nouri, H. Injection of fresh river water into a saline floodplain aquifer as a salt interception measure in a semi-arid environment. *Ecol. Eng.* **2015**, *75*, 308–322, doi:10.1016/j.ecoleng.2014.11.014.

22. Moeck, C.; Brunner, P.; Hunkeler, D. The influence of model structure on groundwater recharge rates in climate-change impact studies. *Hydrogeol. J.* **2016**, *24*, 1171–1184, doi:10.1007/s10040-016-1367-1.

23. Schilling, O.S.; Doherty, J.; Kinzelbach, W.; Wang, H.; Yang, P.N.; Brunner, P. Using tree ring data as a proxy for transpiration to reduce predictive uncertainty of a model simulating groundwater–surface water–vegetation interactions. *J. Hydrol.* **2014**, *519*, 2258–2271, doi:10.1016/j.jhydrol.2014.08.063.

24. Sulis, M.; Paniconi, C.; Marrocu, M.; Huard, D.; Chaumont, D. Hydrologic response to multimodel climate output using a physically based model of groundwater/surface water interactions. *Water Resour. Res.* **2012**, *48*, doi:10.1029/2012WR012304.

25. Fatichi, S.; Vivoni, E.R.; Ogden, F.L.; Ivanov, V.Y.; Mirus, B.; Gochis, D.; Downer, C.W.; Camporese, M.; Davison, J.H.; Ebel, B.; et al. An overview of current applications, challenges, and future trends in distributed process-based models in hydrology. *J. Hydrol.* **2016**, *537*, 45–60, doi:10.1016/j.jhydrol.2016.03.026.

26. Piras, M.; Mascaro, G.; Deidda, R.; Vivoni, E.R. Quantification of hydrologic impacts of climate change in a Mediterranean basin in Sardinia, Italy, through high-resolution simulations. *Hydrol. Earth Syst. Sci.* **2014**, *18*, 5201–5217, doi:10.5194/hess-18-5201-2014.

27. Azarnivand, A.; Camporese, M.; Alaghmand, S.; Daly, E. Simulated response of an intermittent stream to rainfall frequency patterns. *Hydrol. Process.* **2020**, *34*, 615–632, doi:10.1002/hyp.13610.

28. Maxwell, R.M.; Kollet, S.J. Interdependence of groundwater dynamics and land-energy feedbacks under climate change. *Nat. Geosci.* **2008**, *1*, 665, doi:10.1038/ngeo315.

29. Meixner, T.; Manning, A.H.; Stonestrom, D.A.; Allen, D.M.; Ajami, H.; Blasch, K.W.; Brookfield, A.E.; Castro, C.L.; Clark, J.F.; Gochis, D.J.; et al. Implications of projected climate change for groundwater recharge in the western United States. *J. Hydrol.* **2016**, *534*, 124–138, doi:10.1016/j.jhydrol.2015.12.027.

30. Touhami, I.; Chirino, E.; Andreu, J.M.; Sánchez, J.R.; Moutahir, H.; Bellot, J. Assessment of climate change impacts on soil water balance and aquifer recharge in a semiarid region in south east Spain. *J. Hydrol.* **2015**, *527*, 619–629, doi:10.1016/j.jhydrol.2015.05.012.

31. Barron, O.; Silberstein, R.; Ali, R.; Donohue, R.; McFarlane, D.J.; Davies, P.; Hodgson, G.; Smart, N.; Donn, M. Climate change effects on water-dependent ecosystems in south-western Australia. *J. Hydrol.* **2012**, *434-435*, 95–109, doi:10.1016/j.jhydrol.2012.02.028.

32. Ali, R.; McFarlane, D.; Varma, S.; Dawes, W.; Emelyanova, I.; Hodgson, G. Potential climate change impacts on the water balance of regional unconfined aquifer systems in south-western Australia. *Hydrol. Earth Syst. Sci.* **2012**, *16*, 4581–4601, doi:10.5194/hess-16-4581-2012.

33. DHI. *MIKE SHE User Manual Reference Guide*; DHI Groups: Århus Denmark 2014; Volume 2, pp. 299–308.

34. Racsko, P.; Szeidl, L.; Semenov, M. A serial approach to local stochastic weather models. *Ecol. Model.* **1991**, *57*, 27–41, doi:10.1016/0304-3800(91)90053-4.

35. Semenov, M.A.; Barrow, E.M. Use of a stochastic weather generator in the development of climate change scenarios. *Clim. Chang.* **1997**, *35*, 397–414, doi:10.1023/A:1005342632279.

36. Dean, J.; Camporese, M.; Webb, J.; Grover, S.; Dresel, P.; Daly, E. Water balance complexities in ephemeral catchments with different land uses: Insights from monitoring and distributed hydrologic modeling. *Water Resour. Res.* **2016**, *52*, 4713–4729.

37. Allen, R.G.; Pereira, L.S.; Raes, D.; Smith, M. Crop evapotranspiration-Guidelines for computing crop water requirements-FAO Irrigation and drainage paper 56. *Fao Rome* **1998**, *300*, D05109.

38. Dean, J.; Webb, J.; Jacobsen, G.; Chisari, R.; Dresel, P. A groundwater recharge perspective on locating tree plantations within low-rainfall catchments to limit water resource losses. *Hydrol. Earth Syst. Sci.* **2015**, *19*, 1107–1123.

39. Camporese, M.; Daly, E.; Dresel, P.E.; Webb, J.A. Simplified modeling of catchment-scale evapotranspiration via boundary condition switching. *Adv. Water Resour.* **2014**, *69*, 95–105.

40. Pereira, J.M.; Tomé, M.; Carreiras, J.M.; Tomé, J.A.; Pereira, J.S.; David, J.S.; Favião, A.M. Leaf area estimation from three allometrics in Eucalyptus globulus plantations. *Can. J. For. Res.* **1997**, *27*, 166–173.

41. Taylor, K.E.; Stouffer, R.J.; Meehl, G.A. An Overview of CMIP5 and the Experiment Design. *Bull. Am. Meteorol. Soc.* **2011**, *93*, 485–498, doi:10.1175/BAMS-D-11-00094.1.

42. Van Vuuren, D.P.; Edmonds, J.; Kainuma, M.; Riahi, K.; Thomson, A.; Hibbard, K.; Hurtt, G.C.; Kram, T.; Krey, V.; Lamarque, J.-F.; et al. The representative concentration pathways: An overview. *Clim. Chang.* **2011**, *109*, 5, doi:10.1007/s10584-011-0148-z.

43. McGregor, J.L.; Dix, M.R. An updated description of the conformal-cubic atmospheric model. In *High Resolution Numerical Modelling of the Atmosphere and Ocean*; Springer: New York, NY, USA, 2008; pp. 51–75, doi:10.1007/978-0-387-49791-4_4.

44. Timbal, B.; McAveney, B.J. An analogue-based method to downscale surface air temperature: Application for Australia. *Clim. Dyn.* **2001**, *17*, 947–963, doi:10.1007/s003820100156.

45. Whetton, P.; Hennessy, K.; Clarke, J.; McInnes, K.; Kent, D. Use of Representative Climate Futures in impact and adaptation assessment. *Clim. Chang.* **2012**, *115*, 433–442.

46. Clarke, J.M.; Whetton, P.H.; Hennessy, K.J. Providing application-specific climate projections datasets: CSIRO's Climate Futures Framework. In Proceedings of the MODSIM 2011—19th International Congress on Modelling and Simulation—Sustaining Our Future: Understanding and Living with Uncertainty, Perth, Australia, 12–16 December 2011; pp. 2683–2690.

47. CSIRO. Bureau-of-Meteorology. Climate Change in Australia. Availabe online: www.climatechangeinaustralia.gov.au (accessed on 24 August 2017).

48. Riahi, K.; Rao, S.; Krey, V.; Cho, C.; Chirkov, V.; Fischer, G.; Kindermann, G.; Nakicenovic, N.; Rafaj, P. RCP 8.5—A scenario of comparatively high greenhouse gas emissions. *Clim. Chang.* **2011**, *109*, 33, doi:10.1007/s10584-011-0149-y.

49. Eyring, V.; Bony, S.; Meehl, G.A.; Senior, C.A.; Stevens, B.; Stouffer, R.J.; Taylor, K.E. Overview of the Coupled Model Intercomparison Project Phase 6 (CMIP6) experimental design and organization. *Geosci. Model Dev.* **2016**, *9*, 1937–1958.

50. Thomson, A.M.; Calvin, K.V.; Smith, S.J.; Kyle, G.P.; Volke, A.; Patel, P.; Delgado-Arias, S.; Bond-Lamberty, B.; Wise, M.A.; Clarke, L.E.; et al. RCP4.5: A pathway for stabilization of radiative forcing by 2100. *Clim. Chang.* **2011**, *109*, 77, doi:10.1007/s10584-011-0151-4.

51. Semenov, M.A.; Stratonovitch, P. Use of multi-model ensembles from global climate models for assessment of climate change impacts. *Clim. Res.* **2010**, *41*, 1–14.

52. Semenov, M.A.; Brooks, R.J.; Barrow, E.M.; Richardson, C.W. Comparison of the WGEN and LARS-WG stochastic weather generators for diverse climates. *Clim. Res.* **1998**, *10*, 95–107.

53. Von Salzen, K.; Scinocca, J.F.; McFarlane, N.A.; Li, J.; Cole, J.N.S.; Plummer, D.; Verseghy, D.; Reader, M.C.; Ma, X.; Lazare, M.; et al. The Canadian Fourth Generation Atmospheric Global Climate Model (CanAM4). Part I: Representation of Physical Processes. *Atmos. Ocean* **2013**, *51*, 104–125, doi:10.1080/07055900.2012.755610.

54. Collins, W.J.; Bellouin, N.; Doutriaux-Boucher, M.; Gedney, N.; Halloran, P.; Hinton, T.; Hughes, J.; Jones, C.D.; Joshi, M.; Liddicoat, S.; et al. Development and evaluation of an Earth-System model—HadGEM2. *Geosci. Model Dev.* **2011**, *4*, 1051–1075, doi:10.5194/gmd-4-1051-2011.

55. Watanabe, M.; Suzuki, T.; O'ishi, R.; Komuro, Y.; Watanabe, S.; Emori, S.; Takemura, T.; Chikira, M.; Ogura, T.; Sekiguchi, M.; et al. Improved Climate Simulation by MIROC5: Mean States, Variability, and Climate Sensitivity. *J. Clim.* **2010**, *23*, 6312–6335, doi:10.1175/2010JCLI3679.1.